NJC

ROYAL SOCIETY OF CHEMISTRY

PAPER

View Article Online
View Journal | View Issue

Cite this: *New J. Chem.*, 2024, **48**, 4617

Synthesis of glycerol carbonate using Li/Mg/K modified zeolite beta: a kinetic study†

Priyanka Gautam,[a] Sanghamitra Barman *[b] and Amjad Ali *[ac]

Received 3rd November 2023,
Accepted 8th February 2024

DOI: 10.1039/d3nj05074b

rsc.li/njc

In the present investigation, glycerol and dimethyl carbonate were transesterified using a Li/Mg/K modified zeolite beta catalyst to synthesize glycerol carbonate. The various prepared zeolite catalysts were characterized using XRD, FE-SEM, EDS, HR-TEM, XPS, and DLS techniques. Many tests were conducted to optimize the reaction conditions to obtain the highest yield of glycerol carbonate by changing the catalyst concentration (5–20 wt%), glycerol-to-dimethyl carbonate mole ratio (1 : 2–1 : 6), and reaction temperature (65–105 °C). A maximum of 81.48% glycerol carbonate was obtained under optimized reaction conditions (a glycerol : dimethyl carbonate mole ratio of 1 : 5, a $Li_{20}\beta$ dosage of 10 wt% w.r.t. GLY, a temperature of 95 °C, and a time of 5 h). The experimental data followed second-order reaction kinetics with an activation energy of 34.60 kJ mol^{-1}.

1. Introduction

The increasing consumption of fossil fuels leads to increased global warming. This increase needs to be controlled, and many countries all over the world have taken many serious steps to minimize this global warming threat. Renewable fuels can be used to replace the usage of fossil fuels in our day-to-day lives. Biodiesel (BD) is the best substitute among all renewable resources. The growth of BD capacity has increased 5 times from 2006 to 2020.[1] BD, at a commercial scale, is obtained by transesterifying a variety of triglycerides, such as *Jatropha curcas*, used cooking oils, yellow grease, animal fats, *etc.*, with methanol or ethanol. This reaction, along with fatty acid methyl esters (FAME), commonly known as BD, also yielded crude glycerol (GLY) as a by-product[2–7] which is around 10 wt% of the BD production.[8]

The largest GLY manufacturer is in Europe, producing nearly 2.5 million tons of GLY per year, which is estimated to triple by 2030.[9] The estimated global market is predicted to be around US $150 billion by the end of the year 2024.[10] The rapid increase in the production of BD in the last few years has dropped the global price of GLY from US$ 0.27–0.41 per pound to US$ 0.04–0.09 per pound.[11] Thus, it becomes crucial to convert this crude GLY to value-added chemicals and fuel additives like esters, ethers, acrolein, glyceric acid, propanediol, acetins, glycerol carbonate (GC), *etc.*[12,13] Out of all the GLY derivatives, GC (4-hydroxymethyl-1,3-dioxolane-2-one) has got more attention as it is a green compound of the century, biodegradable, less toxic with a high boiling point, and low flammability properties. It is extensively used in the manufacturing of plastic, paint, biological lubricants, and fibers, as a solvent in the cosmetic industries, and as an electrolyte for lithium-ion batteries.[14] Moreover, it plays a significant role in the synthesis of polymers and glycidol.[15] The Transparency Market Research report says that the global market for GC will hike at around 7% per year and reach US$ 2.4 billion by 2030.

Various direct and indirect catalytic pathways have been designed to convert GLY to value-added products shown in Scheme 1.[16] Among all the pathways, the indirect synthesis pathway involved carboxylation of phosgene and transesterification using alkylene and dialkyl carbonate.[17] GC synthesized *via* these pathways showed a high yield as nucleophilic carbon of the carbonate group reacts with the hydroxyl group of the GLY. The direct synthesis pathways were used earlier and were stopped due to the hazardous nature of carbon monoxide. These days, Huntsman Corporation is using oxidative carbonylation for the production of GC. Carbonates like alkyl carbonates and dimethyl carbonates (DMC) can also be used as a source of carbonate for the reaction. Direct carboxylation of GLY with DMC is the potential pathway for GC synthesis under mild reaction conditions. This pathway not only gives maximum conversion of GLY and yield of GC but also provides easy separation as there is quite a large difference in the boiling point of reactants and the product obtained.[18]

A basic homogeneous as well as heterogeneous catalyst is required to synthesize GC from GLY *via* transesterification

[a] *Department of Chemistry and Biochemistry, Thapar Institute of Engineering and Technology, Patiala-147004, India. E-mail: amjadali@thapar.edu*
[b] *Department of Chemical Engineering, Thapar Institute of Engineering and Technology, Patiala-147004, India. E-mail: sbarman@thapar.edu*
[c] *TIET-VT Center of Excellence for Emerging Materials, Thapar Institute of Engineering and Technology, Patiala-147004, India*

† Electronic supplementary information (ESI) available. See DOI: https://doi.org/10.1039/d3nj05074b

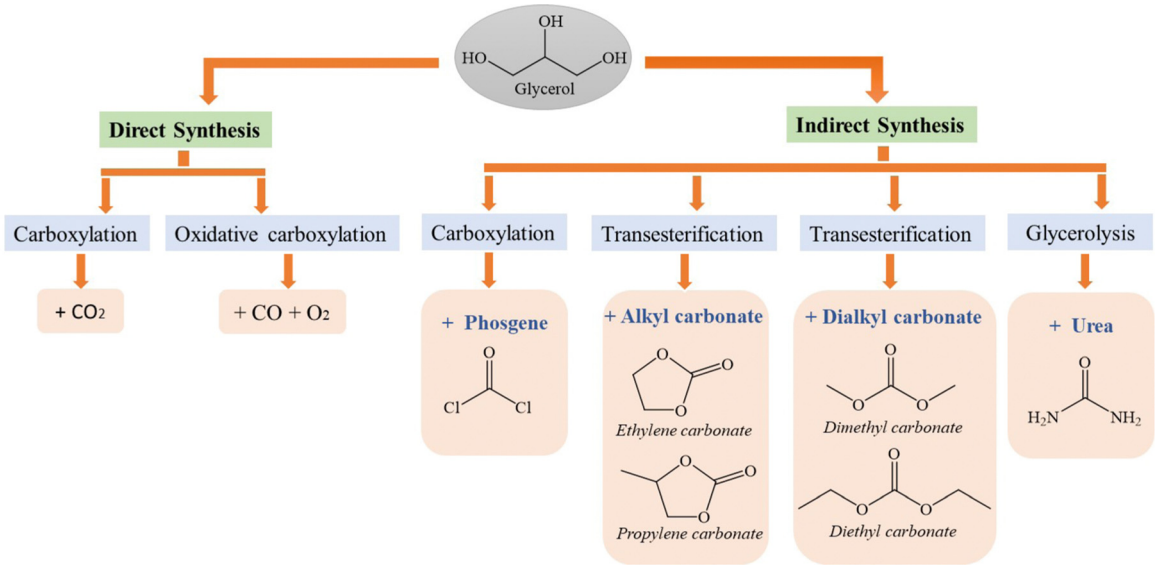

Scheme 1 Various pathways for the synthesis of GC.

reaction.[19] Many homogeneous catalytic systems are reported in the literature, *viz.*, K_2CO_3,[20] trimethylamine,[21] ionic liquids,[22] alkali and alkaline earth metal hydroxides.[23] Although excellent results are obtained from these catalysts, they also have disadvantages like difficulties in separation from the reaction mixture and impossibility of its reuse. To conquer these drawbacks, heterogeneous catalysts were adopted in the transesterification reaction. It is very simple to remove these catalysts from the reaction medium and reuse them multiple times. A variety of basic heterogeneous catalysts have been used by researchers in the past few decades, *viz.*, MgO,[24,25] CaO,[26] CaO-ZrO_2,[27] Mg/ZnO,[28] Ca–Al hydrocalumite,[29] mixed oxides,[30–34] $NaAlO_2$ doped CaO,[35] Na_2SiO_3,[36] oil palm empty fruit bunch ash,[37] Ti-SBA-15,[38] Ni/FA,[39] K-TUD-1,[40] Co/MCM-41,[41] K-zeolite,[42] anion exchange resins,[43] Na-based zeolites,[44] trisodium phosphate,[45] Sr-Al,[46] *etc.* Catalysts like metal oxides and mixed metal oxides show high GC yield but also leaching problems that degrade their reusability properties. Basic sites of the catalyst are responsible for the initiation of the reaction. The catalyst made with metals like lithium (Li), sodium (Na), potassium (K), cerium (Ce), molybdenum (Mo), *etc.* gives a good yield of GC. Lithium nitrate shows a strong ion size effect of all alkali metals, which is responsible for creating strong basic sites. The literature shows some catalysts with lithium metal such as alkali metal silicates (Li, Na, K),[47] Li/CaO–La_2O_3,[48] Li/Mg composites,[49] $LiNO_3/Mg_4AlO_{5.5}$,[50] Li/ZnO,[51] Li/MCM-41,[52] Li/CFA,[53] Li_4SiO_4,[54] Li-oil palm ash zeolite,[55] and Li/ZrO_2[13] used for the transesterification reaction of GLY and DMC. Very less literature is available on the transesterification reaction using zeolite and modified zeolite.[56] A comparison of the presently used catalyst and other catalysts reported in the last 10 years is shown in Table 1. Hence, the present work is focused on zeolite beta modified with alkali and alkaline earth metals like Li, Mg, and K for synthesizing GC *via* the transesterification reaction of GLY and DMC under mild conditions. The main purpose of using alkali and alkaline earth metals with zeolite is that they provide several benefits like reducing support acidity, improving physiochemical properties, and increasing the basicity of oxygen atoms in the zeolite framework. Various Li modified zeolite beta catalysts were synthesized and the best-performing Li modified zeolite was compared with Mg and K modified zeolite beta. ^{1}H NMR spectroscopy was performed for the quantification of GC formed and the remaining GLY in the reaction. The kinetic study of the reaction was also performed. A comparison with previously reported zeolites is presented in Table S1 (ESI†).

2. Experimental section

2.1. Materials

The ammonium form of zeolite beta was purchased from Alfa Aeser Company. DMC was procured from Spectrochem Pvt. Ltd (India). Lithium nitrate ($LiNO_3$), magnesium nitrate ($Mg(NO_3)_2$), potassium nitrate (KNO_3), GLY, methanol, ethyl acetate, and potassium permanganate ($KMnO_4$) were purchased from LobaChemie Ltd, India. Sigma-Aldrich (USA) provided the D_2O used in the ^{1}H and ^{13}C NMR experiments. All of the reagents were used as they were originally obtained from the company.

2.2. Catalyst synthesis

The ammonium form of zeolite was converted to the hydrogen form by calcining it at 350 °C for 3 h. By this step, the H-form of zeolite beta was prepared and was ready to be used in the reaction. A 30 mL solution of lithium nitrate salt was prepared at a particular concentration and mixed with 1 g of zeolite beta. The above-mentioned solution was continuously mixed at 35 °C for 4 h and then filtered. It was then oven-dried at 120 °C for 12 h. Finally, the calcination process of the obtained white powder was done at 700 °C for 4 h. Thus, impregnation of lithium in the zeolite was done using this procedure. Similarly, other metals like Mg and K were impregnated in the zeolite

Table 1 Comparison of the catalytic performance of different catalysts for the synthesis of GC

Catalyst	Catalyst loading	Reaction conditions	Yield (%)	GLY conversion (%)	Selectivity of GC (%)	Reusability	Ref.
$LiNO_3/Mg_4AlO_{5.5}$	5 wt%	1 : 3, 80 °C, 1.5 h	96.28	100	—	—	50
Trisodium phosphate	3 wt%	1 : 2, 70 °C, 1 h	99.5	99.5	100	9	46
$Li/CaO–La_2O_3$	5 wt%	1 : 15, 60 °C, 2.5 h	—	96.3%	—	5	48
Na_2SiO_3-200	0.9 g	1 : 4, 75 °C, 2.5 h	91.8	97.7	94.0	5	36
MAZ	0.1 g	3 : 1 : 1, 75 °C, 90 min	94	—	—	—	30
Li–OPAZ	2 wt%	2 : 1, 343 K, 90 min	98.0	100	—	5	55
Li/ZnO	5 wt%	1 : 2, 95 °C, 4 h	96.12	97.40	—	4	51
Sr–Al	3 wt%	1 : 2, 70 °C, 1 h	99.4	99.4	100	5	47
BaO	5 wt%	1 : 3; 120 °C, 1.5 h, DMF	68.6	98	70	—	33
CaO	3 wt%	1 : 3, 80 °C, 2 h	92.1	—	—	—	26
$Li–La_2O_3$	3.3 wt%	1 : 3, 85 °C, 3 h	94.4	93.7	92.1	4	49
MgO	0.3 g	1 : 3, 90 °C, 2 h	99	—	—	3	25
Ti-SBA-15	5.5 wt%	1 : 5, 100 °C, 2 h	—	—	—	3	38
$MgO–CeO_2$	0.3 g	1 : 5, 90 °C, 90 min	86.0	—	100	—	31
$NaAlO_2$	30 wt%	1 : 4, 70 °C, 2 h	85	85	100	5	35
EFBA	5 wt%	1 : 5, 90 °C, 45 min	95.6	—	—	4	37
MgO-500	300 mg	1 : 5, 90 °C, 100 min	93.0	—	93.0	5	24
Li/ZrO_2	5 wt%	1 : 3, 95 °C, 2 h	91.0	91.0	100	4	13
K/TUD-1	6 wt%	1 : 5, 90 °C, 2.5 h	91.53	98.0	—	4	40
$CaO–ZrO_2$	0.3 g	0.6 : 1, 90 °C, 2 h	—	97.0	93.0	—	27
Mg/ZnO	3 wt%	4 : 1, 80 °C, 2 h	90.17	98.40	98.37	6	28
$CoFe_2O_4$@(CaO–ZnO)	46 mg	1 : 5, 85 °C, 2.5 h	96.9	97.7	99.2	5	34
Ni/FA	7.5%	1 : 12, 550 °C, 220 min	—	98.6	—	—	39
Ca/Al	0.15 g	1 : 3, 70 °C, 3 h	—	93	97	6	29
Li/CFA	2 wt%	—, 90 °C, 2 h	91.72	96.33	—	4	53
Li/MCM-41	4 wt%	1 : 3, 90 °C, 3 h	93.14 ± 2.52%	99 ± 1.89%	—	4	52
Dowex 1 × 2	2 wt%	2 : 1, 105 °C, 5 h	43	95.0	45.5	—	44
Co/MCM-41	6 wt%	1 : 3, 90 °C, 2 h	81.6	96.7	—	4	41
Mg_1Zr_2-HT	3 wt%	1 : 5, 90 °C, 60 min	96.0	91.3	95.1	4	32
Li/Mg	4 wt%	3 : 1, 80 °C, 2 h	90.61	92.05	99.44	4	49
$Li_{20}\beta$	10 wt%	1 : 5, 95 °C, 5 h	81.48	—	100	5	Present work

using the same procedure. Different concentrations of metal-modified zeolite are designated as $Li_x\beta$, where x represents the metal content in wt%, M represents the loaded metal and β stands for zeolite beta. The diagrammatic representation of the modification of zeolite beta is shown in Fig. S1 (ESI†).

2.3. Characterization

A series of Li-modified zeolites were prepared using the wet-impregnation method. Various characterization techniques were used to check the modification of zeolite beta. The powder XRD was carried out using Cu-Kα (λ = 0.15406 nm) radiation on a Rigaku SmartLab SE instrument with an angle range of 5 to 80°. Field emission scanning electron microscopy (FE-SEM) of various catalysts was performed on a Zeiss instrument. X-ray photoelectron spectroscopy (XPS) was carried out using a Thermo Fisher ESCALAB Xi+ instrument to identify the elements present in zeolite samples. DLS of the pure and $Li_{20}\beta$ zeolite samples was performed on a zeta potential analyzer (model: ZEN 3600, Malvern, UK). HR-TEM images of pure and $Li_{20}\beta$ zeolite samples were obtained from a JEOL JEM 2100 PLUS instrument. A JEOL ECS-400 (400 MHz) instrument was used to record the Fourier transform-nuclear magnetic resonance (FT-NMR) and ^{13}C-NMR spectra of GLY and GC having tetramethyl silane (TMS) as an internal reference. A QTOF mass spectrometer with UPLC (XEVO G2 XS) was used to calculate the mass of the product and leftover reactant in the reaction mixture. KBr pellet FTIR (Fourier transform infrared) was performed on an IRTracer-100 instrument.

2.4. Synthesis of GC

GLY and DMC were transesterified with a metal-modified zeolite beta catalyst to produce GC. The reactants and catalyst were taken in a 50 mL two-necked round bottom flask (RBF), having a thermocouple attached, a water-cooling condenser, a magnetic stirrer, and an oil bath. The two-necked RBF was placed inside the oil bath. The magnetic stirrer and thermocouple were inserted into the oil bath to monitor the reaction temperature. In a typical reaction, 0.054 and 0.107 moles of GLY and DMC, respectively, were added into the RBF, followed by the addition of a specific amount of the desired catalyst. The reaction was carried out at 95 °C for 4 h. Aliquots were taken after every hour to check the performance of the catalyst and its feasibility for the scale-up reaction where its reusability was checked. Thin layer chromatography (TLC) was adopted to observe the reaction progress having ethyl acetate as the mobile phase and aluminium silica plates as the stationary phase. Firstly, TLC was run in ethyl acetate solvent and, after that, it was air-dried and dipped in $KMnO_4$ solution. The brown color of the present components was developed on the TLC plate against the purple color of $KMnO_4$ by gently heating it with a hot air gun. The reaction was stopped when it reached the desired point, and the catalyst was isolated from the reaction

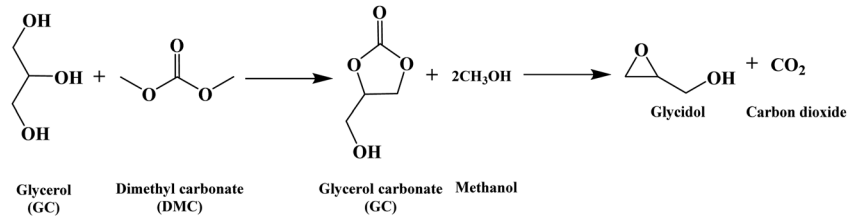

Scheme 2 Synthesis of the by-product (glycidol).

mixture *via* filtration or centrifugation and washed with methanol. It was dried in an oven at 120 °C overnight and recalcined at 700 °C. The remaining reaction mixture containing DMC and methanol was evaporated using a rotary evaporator at 65 °C. A blank reaction was also performed to check the role of Li present in the catalyst. Sometimes, the by-product glycidol is also produced in the reaction shown in Scheme 2.

The GC obtained was then characterized by ^{1}H NMR, ^{13}C NMR, FTIR, and HRMS spectroscopy. A maximum yield of 81.48% of GC was obtained under optimized reaction conditions. ^{1}H NMR (400 MHz, D_2O): δ (ppm) 4.80–4.75 (m, 1H), 4.47–4.42 (t, J = 12 Hz, 1H), 4.23–4.19 (q, 1H), 3.73–3.69 (dd, J = 16,4 Hz, 1H), 3.58–3.55 (m, 1H), 3.54–3.50 (dd, J = 12,4 Hz, 1H), 3.44–3.40 (dd, J = 8,4 Hz, 3H), 3.35–3.31 (dd, J = 12,4 Hz, 3H) (Fig. S2, ESI†). ^{13}C NMR (100 MHz, D_2O): δ (ppm) 157.90, 78.04, 72.05, 66.83, 62.48, 60.91 (Fig. S3, ESI†). FT-IR (KBr) ν_{max} (cm^{-1}): 3246, 2938, 2879, 1767, 1483, 1182, 1052, 921 (Fig. S4, ESI†). HRMS (ESI-TOF): (m/z) [GC] calculated for $C_4H_6O_4$: 118.0498, found: 118.0502 (Fig. S5, ESI†).

The obtained reaction mixture containing GC and GLY was then quantified using ^{1}H NMR spectroscopy shown in Fig. 1 using eqn (1):

$$\%C_{GC} = 100 \times \left(\frac{I_{c_1}}{I_d + I_{c_2}}\right). \quad (1)$$

where $\%C_{GC}$ is the percentage of GC, I_{c_1} is one of the methylene protons' (c_1) integral of non-superimposed doublets of GC, and $I_d + I_{c_2}$ is the complete integral of the methylene proton (c_2) doublet of the superimposed protons of GC and the methine proton (d) of GLY.

3. Results and discussion

3.1. Catalyst characterization

3.1.1. X-ray diffraction (XRD). Fig. 2a shows the XRD patterns for the comparison of alkali and alkaline earth metals such as Li, Mg and K. The XRD patterns of zeolite beta and $Li_{20}\beta$ zeolite with different phases that are formed are shown in Fig. 2b. The characteristic peaks of $LiAlO_2$ (JCPDS card no. 38-1464), Li_2SiO_3 and Li_4SiO_4 are shown in the graph.[54,57] It is

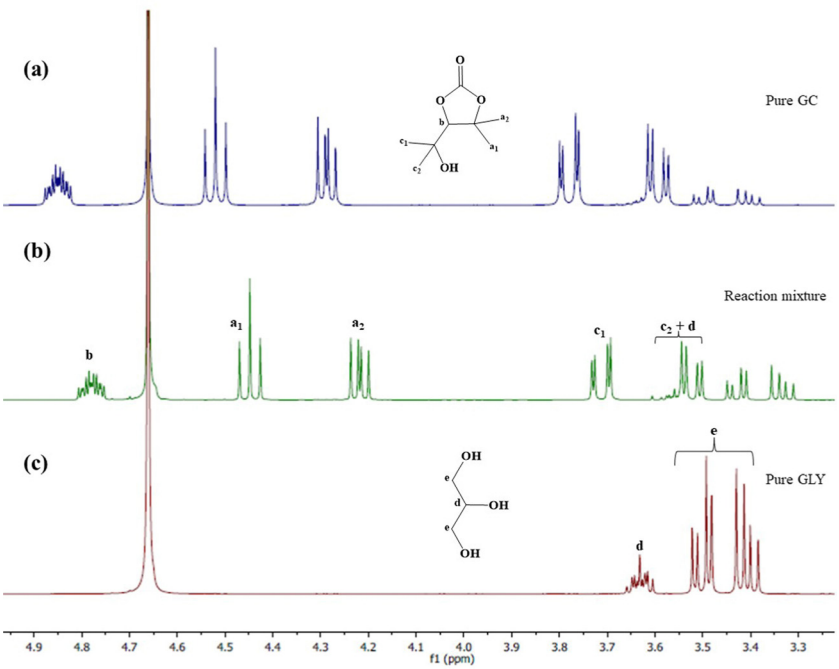

Fig. 1 ^{1}H NMR spectra of (a) pure GC, (b) the reaction mixture under optimized reaction conditions, and (c) pure GLY.

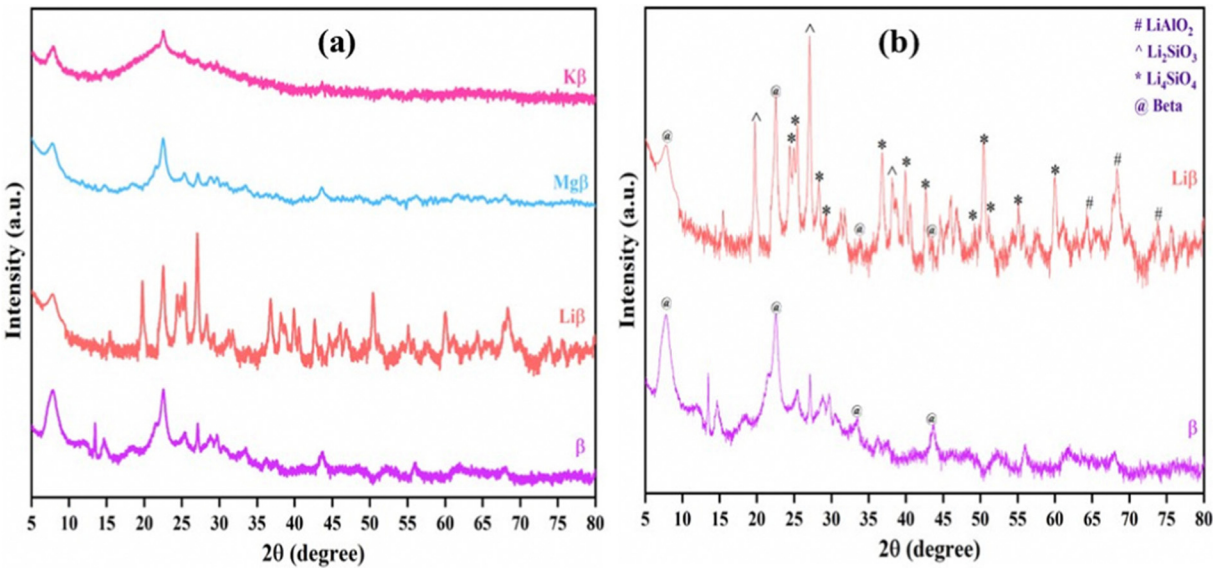

Fig. 2 (a) Comparison of the XRD patterns of beta, Li, Mg, and K modified beta zeolite and (b) XRD patterns of different phases of Li with alumina and silica.

clearly visible from the XRD patterns that there is no change in the structure of the zeolite framework even after the modification with active metal.

3.1.2. Field emission scanning electron microscopy (FE-SEM). The morphological images of the parent zeolite beta and Li, Mg and K modified zeolite beta are shown in Fig. 3. The figure displays the spherical shapes of parent zeolite beta, which becomes slightly distorted after modification with Li, Mg and K as illustrated in Fig. 3b–d. The particles have spherical shapes but do not have well-defined edges. The metal modified zeolites also show a spherical structure, which confirms that the basic morphology of the zeolite remains the same even after modification. The EDS spectra of metal (Li, Mg, K) modified zeolite are shown in Fig. 4. The spectra revealed that a good amount of metal is loaded on the zeolite beta. As Li cannot be detected in SEM/EDS, no peak of Li is observed in the EDS spectra of $Li_{20}\beta$ zeolite.

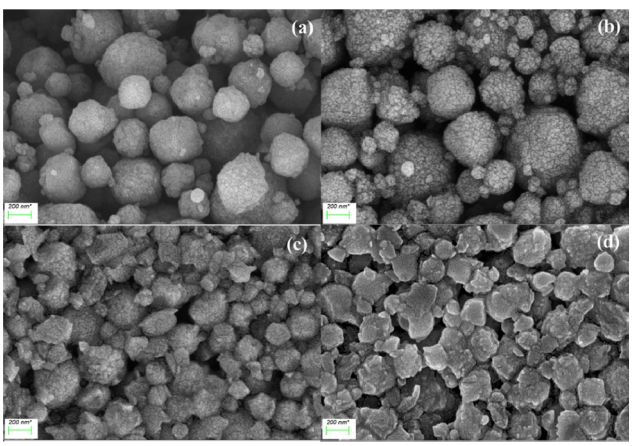

Fig. 3 FE-SEM images of (a) parent zeolite beta and (b) Li modified, (c) Mg modified, and (d) K modified zeolite beta.

3.1.3. High-resolution transmission electron microscopy (HR-TEM). The obtained HR-TEM images of the $Li_{20}\beta$ catalyst are shown in Fig. 5. It is clearly visible from the figure that the $Li_{20}\beta$ catalyst possesses some distortion in the spherical structure. The same results are observed from the FE-SEM images. The average grain diameter and average distance between the two grains come out to be 500 nm and 24.28 nm, respectively.

3.1.4. Dynamic light scattering (DLS). The DLS graphs of beta and $Li_{20}\beta$ zeolite are shown in Fig. 6. DLS was performed to study the size distribution of the beta and $Li_{20}\beta$ catalysts in a suspension. The hydrodynamic size of beta and $Li_{20}\beta$ zeolite from DLS comes out to be 531.326 nm and 605.699 nm, respectively. The increase in the hydrodynamic size of $Li_{20}\beta$ is due to impregnation of Li metal over the surface of the zeolite beta, which results in an increase in its size.

3.1.5. X-ray photoelectron spectroscopy (XPS). XPS of the catalyst ($Li_{20}\beta$) was carried out to study its quantitative elemental composition (Fig. 7a) and the service spectrum of the $Li_{20}\beta$ catalyst shown in Fig. 7b depicts the characteristic peaks of Li (1s), O (1s), Si (2p), and Al (2p).[58–60] The Li 1s spectrum has two deconvoluted peaks with binding energies at 53.9 eV and 54.9 eV as shown in Fig. 7c. The peak at 53.9 eV confirms the Li–O linkage and the peak at 54.9 eV confirms the Li–O–Si linkage. The spectrum of O 1s has been divided into three peaks having binding energies of 530.6, 531.2 and 532.1 eV as shown in Fig. 7d. The peak at 530.6 eV corresponds to the Li–O linkage, the peak at 531.2 eV confirms the presence of the lattice form of oxygen of the zeolite and the peak at 532.1 eV corresponds to the hydroxyl group.[61] The peaks in Fig. 7e at 102.1 and 102.6 eV are the lattice form of Si 2p, which corresponds to Li_xSiO_y and the Si–O–Si linkage, respectively. The spectrum of Al 2p shown in Fig. 7f shows a peak at 74.06 eV, which corresponds to Al–O.

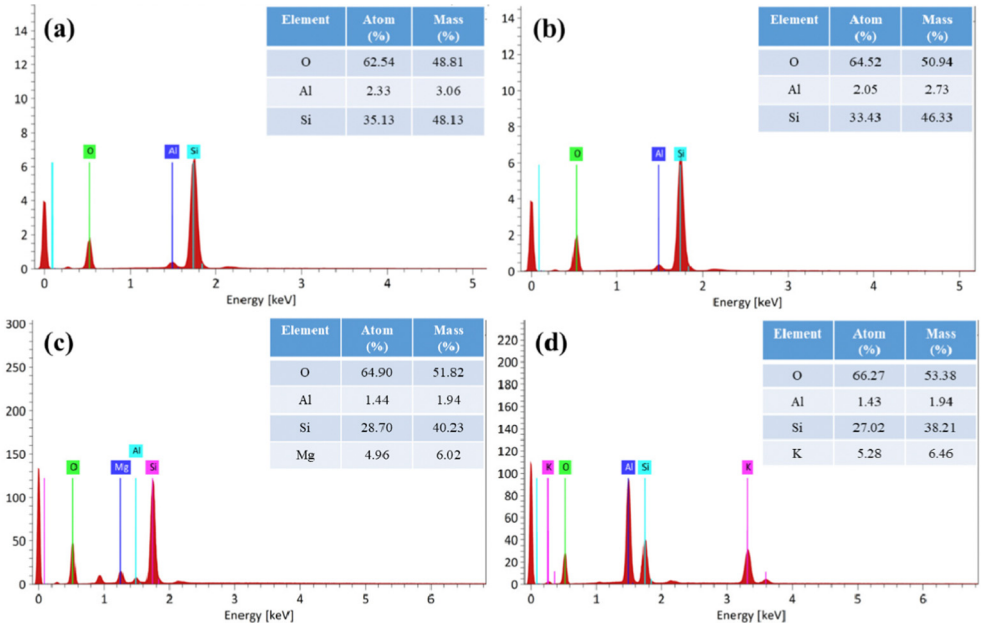

Fig. 4 EDS spectra of (a) parent zeolite beta and (b) Li, (c) Mg, and (d) K modified zeolite beta.

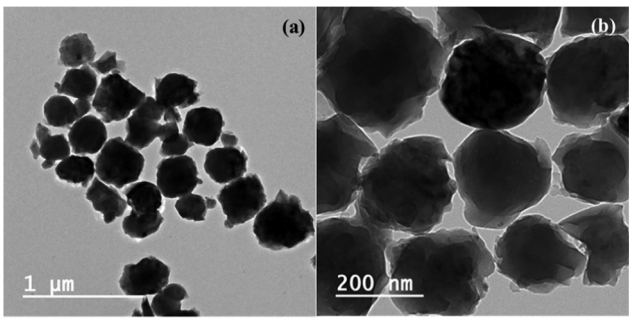

Fig. 5 HR-TEM images of 20Li/beta at (a) lower and (b) higher magnifications.

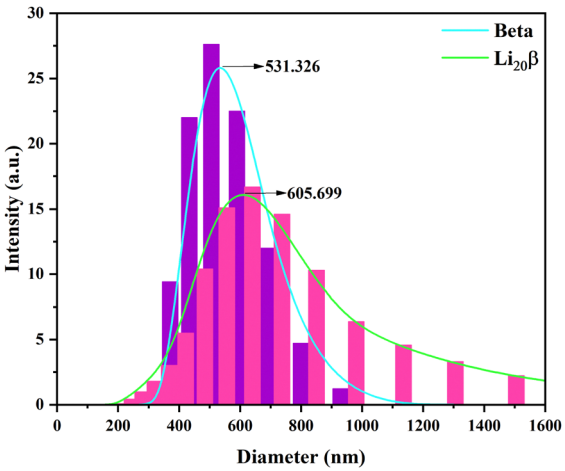

Fig. 6 DLS graph of parent and Li modified zeolite beta.

3.2. Catalyst screening

3.2.1. Selection of metal loading on zeolite beta. In this study, the zeolite beta catalyst was prepared using various alkali and alkaline earth metals such as Li, K, and Mg. In order to determine the catalytic performance of the prepared catalyst, the transesterification reaction of GLY and DMC at a molar ratio of 1 : 5 was performed for 5 h at 95 °C (Fig. 8). The reaction was also performed with the pure zeolite beta catalyst and without any catalyst to check the product formation, *i.e.* GC, in the reaction, and it was observed that no product formation was observed without the catalyst and traces of product in the presence of the pure zeolite beta catalyst. The prepared catalysts exhibited 100% selectivity towards GC without the formation of side products. Among all the prepared catalysts, Li- and K-modified beta zeolite exhibited higher activity. However, while comparing the stability of Li- and K-modified zeolite, Li modified zeolite showed better catalytic activity. Li, K, and Mg modified zeolite beta gave 81.48%, 76.71%, and 59.35% yields of GC, respectively. So, Li/beta zeolite containing 20 wt% Li was selected for all the reactions for the purpose of obtaining the highest GC yield.

3.2.2. Li impregnation over the surface of zeolite. To achieve the maximum yield of GC, zeolite beta was treated with different concentrations of lithium-nitrated solutions using the wet impregnation method. The catalytic activity of the modified zeolite was examined at a dosage of 10 wt% and a reactant mole ratio of 1 : 5 at a temperature of 95 °C for a reaction time of 5 hours. From Fig. 9, it is clearly visible that a 20 wt% loading of Li on zeolite beta gives the maximum GC yield, which is 81.48%. With an increase in the Li metal concentration, the catalytic activity of the zeolite increases. An increase of the GC

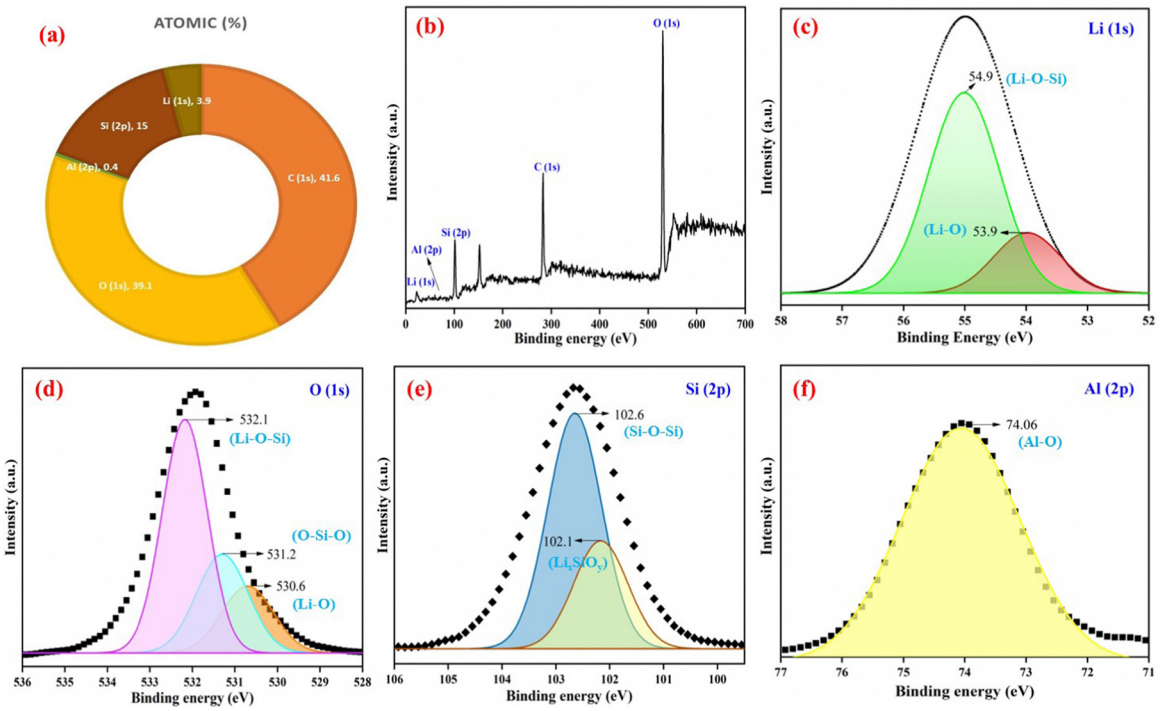

Fig. 7 XPS results: (a) elemental composition, (b) service spectrum, (c) Li (1s), (d) O (1s), (e) Si (2p), and (f) Al (2p).

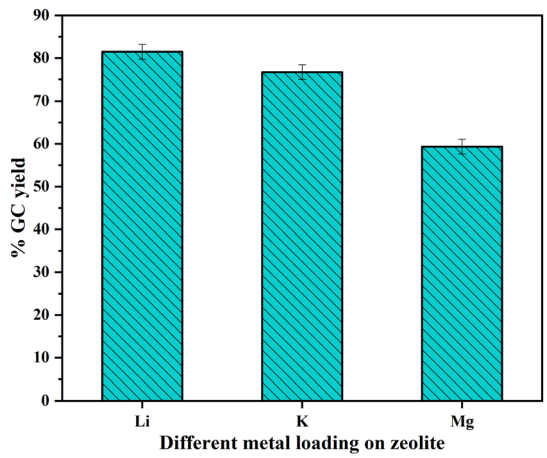

Fig. 8 Effect of different metal contents in zeolite on the yield of GC (reaction conditions: GLY : DMC mole ratio, 1 : 5; $Li_{20}\beta$ dosage, 10 wt% w.r.t. GLY; temperature, 95 °C; time, 5 h).

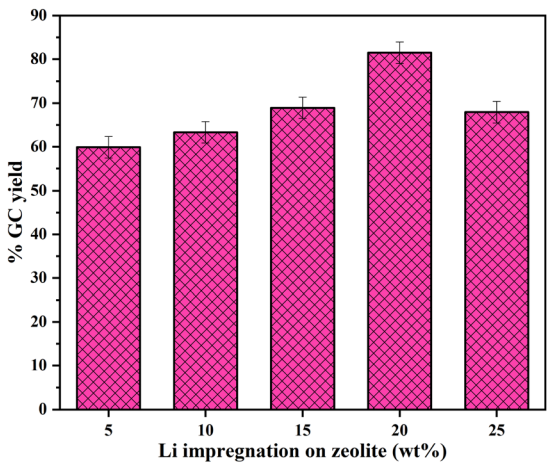

Fig. 9 Effect of Li metal on GC yield (reaction conditions: GLY : DMC mole ratio, 1 : 5; $Li_{20}\beta$ dosage, 10 wt% w.r.t. GLY; temperature, 95 °C; time, 5 h).

yield is observed with 5 to 20 wt% Li loading, and at a 25 wt% catalyst dosage, a decrease in the yield is observed owing to excessive Li clogging the active basic sites present on the zeolite surface, thereby decreasing the yield of GC. Therefore, 20 wt% Li-loaded zeolite beta, named $Li_{20}\beta$ zeolite, was taken for further reactions to achieve the maximum GC yield.

3.3. Effect of reaction parameters

3.3.1. Effect of $Li_{20}\beta$ catalyst dosage on GC yield. The transesterification reaction depends on the presence of the active sites of the basic catalyst which further depends on the type of metal loading on the surface. The more the active sites present, the more the interaction of active sites with the reactants, which leads to high conversion. A negligible reaction occurs in the absence of the catalyst. This is the reason for choosing a good basic catalyst that can cross the activation energy barrier easily. To achieve the maximum GC yield, various catalytic reactions were carried out by changing the catalyst concentration w.r.t. GLY. $Li_{20}\beta$ catalysts with different concentrations, *i.e.* from 5 to 25 wt%, were used and a maximum yield of 81.48% was achieved at 10 wt% (Fig. 10).

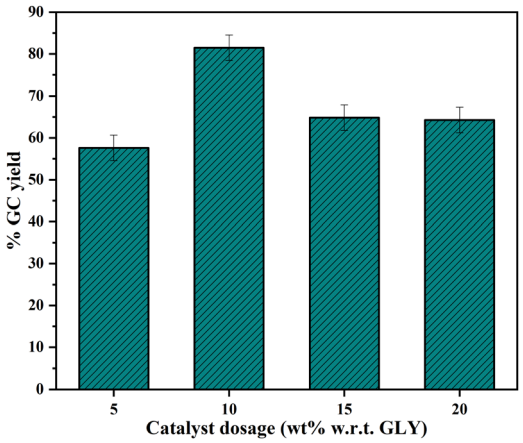

Fig. 10 Effect of catalyst loading w.r.t. GLY (reaction conditions: GLY : DMC mole ratio, 1 : 5; $Li_{20}\beta$ dosage, 10 wt% w.r.t. GLY; temperature, 95 °C; time, 5 h).

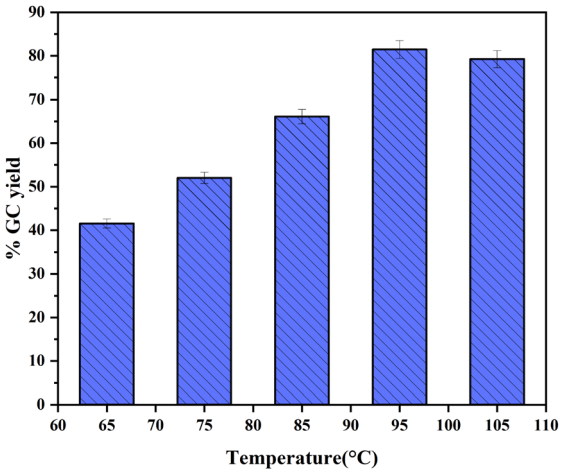

Fig. 12 Effect of catalyst loading w.r.t. GLY (reaction conditions: GLY : DMC mole ratio, 1 : 5; $Li_{20}\beta$ dosage, 10 wt% w.r.t. GLY; temperature, 95 °C; time, 5 h).

However, when the catalyst loading was further increased, it led to a decrease to 64.48% and after that no noticeable change was found in the yield. This could be due to the accumulation of the catalyst particles, which inhibited the mass transfer to the active sites of the catalyst.[41] Hence, a 10 wt% catalyst dosage came out to be the best dosage for the GC synthesis and was selected for optimizing the rest of the parameters for the transesterification reaction.

3.3.2. Effect of the GLY/DMC mole ratio on GC yield. The mole ratio of reactants, *i.e.* GLY/DMC, is one the most important factors affecting the conversion and synthesis of GLY and GC, respectively. In the present work, the mole ratio is varied from 1 : 2 to 1 : 6 for the synthesis of GC as shown in Fig. 11. Initially, as the mole ratio increases, the GC yield increases up to 1 : 5 from 50.71% to 81.48%. After that, a reduction in the GC yield of 67.76% is observed, which may be due to the increase in the immiscibility of the reactants. As we know, GLY is hydrophilic and DMC is hydrophobic in nature; hence, due to the high concentration of DMC in the reaction, the formation of these two phases makes the reaction difficult to proceed, which ultimately decreases the yield of GC.[35]

3.3.3. Effect of reaction temperature on GC yield. Generally, transesterification is a reversible reaction and thus temperature has a significant impact on the progress of a reaction. In general, the higher the reaction temperature, the higher the rate of the reaction and hence the higher the GC yield. To obtain the highest yield of GC, the reaction temperature was varied from 65 °C to 105 °C at a 10 wt% catalyst loading with a mole ratio of 1 : 5 for a 5 hours reaction time as shown in Fig. 12. The same figure represents a prominent rise in the yield of GC from 65 °C to 95 °C. At 95 °C, an 81.48% yield of GC was obtained, the reason being the maximum successful collisions occurred between both reactants at the highest temperature. Beyond this temperature, a slight reduction in the yield was observed, which could be attributed to the decarboxylation of

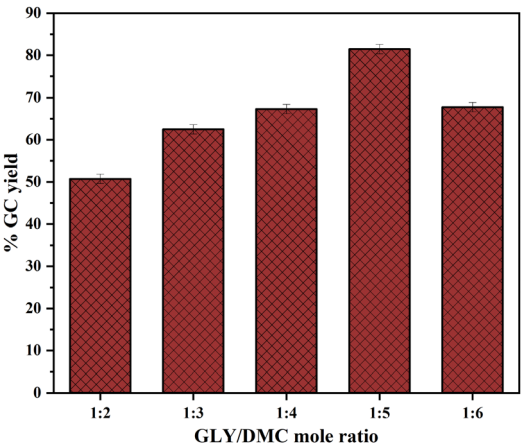

Fig. 11 Effect of catalyst loading w.r.t. GLY (reaction conditions: GLY : DMC mole ratio, 1 : 5; $Li_{20}\beta$ dosage, 10 wt% w.r.t. GLY; temperature, 95 °C; time, 5 h).

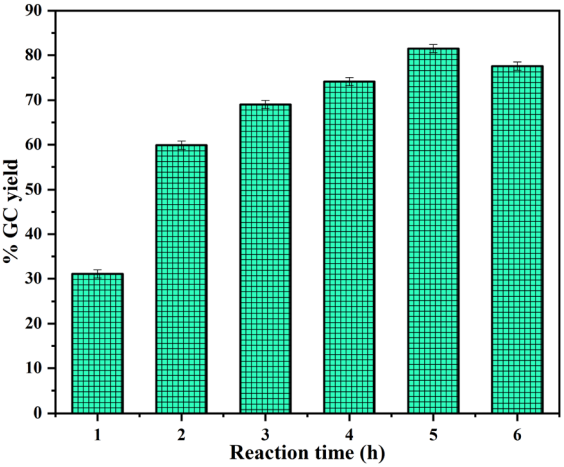

Fig. 13 Effect of catalyst loading w.r.t. GLY (reaction conditions: GLY : DMC mole ratio, 1 : 5; $Li_{20}\beta$ dosage, 10 wt% w.r.t. GLY; temperature, 95 °C; time, 5 h).

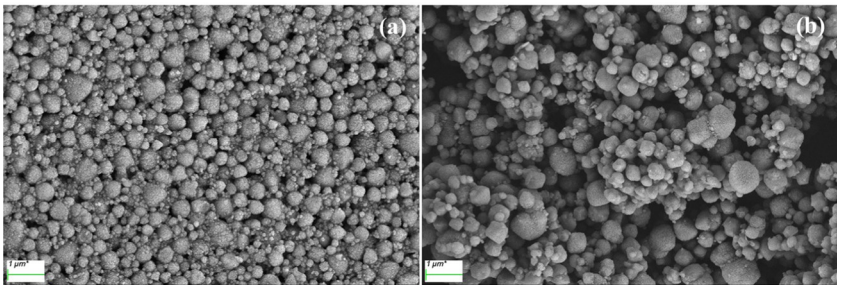

Fig. 14 Comparison of the $Li_{20}\beta$ zeolite (a) before and (b) after the transesterification reaction.

GC into glycidol, which led to ring opening of the GC structure and hence a decrease in the yield of GC.[50]

3.3.4. Effect of reaction time on GC yield. To study the effect of reaction time, the reaction was performed for 6 hours and the observations are shown in Fig. 13. The maximum GC yield was observed in 5 hours under the reaction conditions of a 10 wt% catalyst dosage, a GLY : DMC mole ratio of 1 : 5 at 95 °C. The yield of GC increases from 31.1% to 81.48% in the first five hours of the reaction run. After this, a slight decrease is observed in the sixth hour of the reaction run, which may be due to the excessive basic active sites on the $Li_{20}\beta$ catalyst surface being used to decarboxylate the GC molecule.[51]

3.3.5. Regeneration of the catalyst. The key benefit of using heterogeneous catalysts is its reusability, which makes them more useful at a large scale by lowering the price of the product. The transesterification reaction of GLY with DMC was performed using the catalyst $Li_{20}\beta$ under optimal reaction conditions of a GLY : DMC mole ratio of 1 : 5, a 10 wt% $Li_{20}\beta$ catalyst, a 95 °C reaction temperature and a 5 hours reaction time. The catalyst was regenerated after every cycle. The catalyst was washed with methanol and then oven-dried overnight. After that, it was recalcined at 700 °C. The reactions were performed using the regenerated catalyst and Fig. 14 shows the FE-SEM images of the $Li_{20}\beta$ catalyst before and after the transesterification reaction of GLY with DMC.

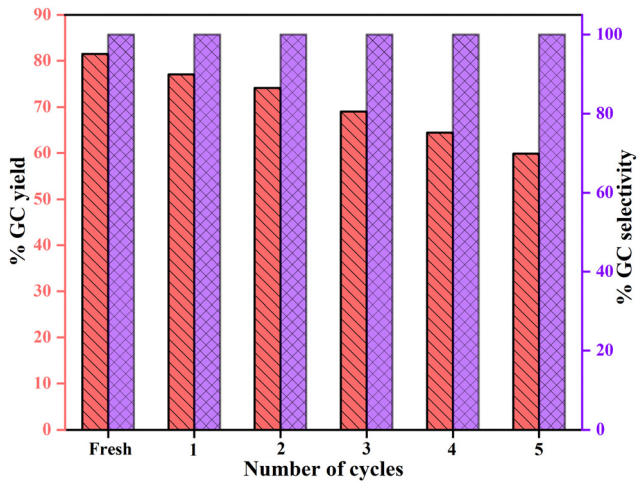

Fig. 15 Reusability of $Li_{20}\beta$ zeolite (reaction conditions: GLY : DMC, 1 : 5; $Li_{20}\beta$ dosage, 10 wt% w.r.t. GLY; temperature, 95 °C; time, 5 h).

3.3.6. Recyclability of the catalyst. The recyclability of the $Li_{20}\beta$ zeolite catalyst was tested by regenerating it as mentioned in the above section under the optimal reaction conditions (GLY : DMC mole ratio of 1 : 5, 10 wt% $Li_{20}\beta$ catalyst, 95 °C reaction temperature and 5 hours reaction time). The $Li_{20}\beta$ zeolite was reused up to five catalytic cycles under the optimal reaction conditions. A gradual decrease in the GC yield was observed from 81.48% to 59.88% for the five cycles and this is shown in Fig. 15. Although a decrease is observed, no side product formation is observed during the reusability process up to five cycles.

4. Reaction kinetics

The kinetics for the transesterification of GLY and DMC has scarcely been reported in the literature as shown in Table S1 (ESI†). The reaction kinetics of transesterification of GLY and DMC was studied in the presence of 10 wt% of $Li_{20}\beta$ zeolite as the best-performing catalyst at temperatures ranging from 65 °C to 95 °C and a 1 : 5 mole ratio of GLY : DMC for a 5 hours reaction time. The aliquots were collected after each hour during the reaction for all the four temperatures. The transesterification reaction of GLY and DMC over $Li_{20}\beta$ zeolite is shown in Scheme 3.

The reaction order was found by plotting rate equations for zero, first and second orders, which are shown in Fig. S6 (ESI†). From all the graphs plotted, the relatively higher value of R^2, which was 0.98, for the second-order reaction rate suggested that the transesterification reaction of GLY and DMC over $Li_{20}\beta$ zeolite followed second-order kinetics as shown in Fig. S6c (ESI†).

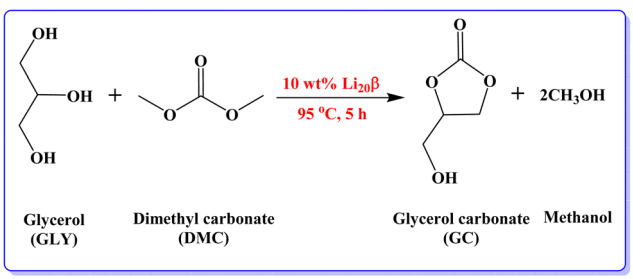

Scheme 3 Synthesis of GC using $Li_{20}\beta$ zeolite.

Table 2 Effect of the rate constant with reaction temperature

Reaction temperature (°C)	Rate constant, k (min^{-1})
65	0.328
75	0.576
85	0.705
95	0.905

Table 3 Activation energy and pre-exponential factor

Activation energy, E_a (kJ mol^{-1})	Pre-exponential factor, A
34.60	7.76×10^4

Table 2 shows the temperature effect on the rate of the reaction and it was confirmed that the k value increases with an increase in the temperature of the reaction. The second-order kinetics at various reaction temperatures is shown in Fig. 16a. The slope of this graph gives different k values for the reaction, which was further applied in the Arrhenius equation to find the activation energy, and the plot of $\ln k$ against $1/T$ is shown in Fig. 16b.

$$k = Ae^{\frac{-E_a}{RT}} \quad (1)$$

$$\ln k = \ln A^{-\frac{E_a}{RT}} \quad (2)$$

where k represents the reaction rate constant, E_a represents the activation energy, A represents the Arrhenius constant, T represents the temperature and R represents the universal gas constant for the reaction.

From Fig. 16b, the activation energy (E_a) comes out to be 34.60 kJ mol^{-1} and the pre-exponential factor (A) comes out to be 7.76×10^4 for the transesterification reaction (Table 3). According to the literature, the activation energy has been reported in the range of 22.012 to 53.77 kJ mol^{-1}.

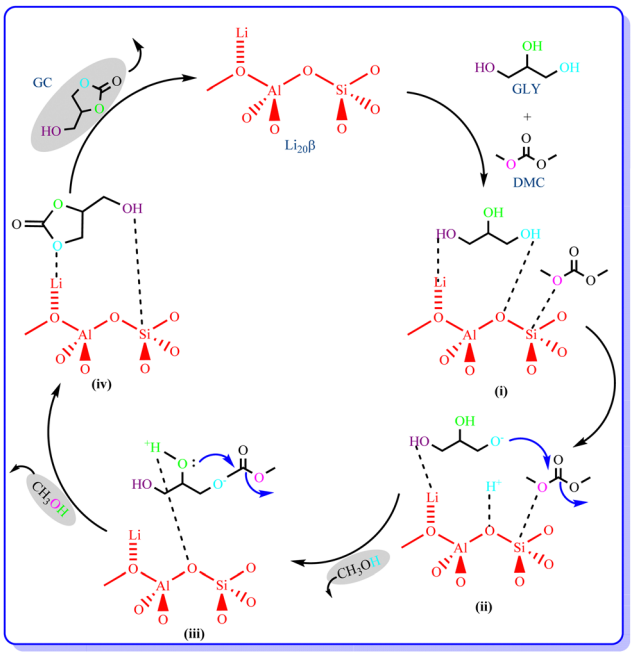

Scheme 4 Plausible mechanism presenting the interaction between GLY, DMC and $Li_{20}\beta$ zeolite.

5. Plausible mechanism

$Li_{20}\beta$ zeolite catalyzed transesterification reaction of GLY with DMC comprises the interaction of the catalyst with both substrates (Scheme 4). Firstly, the basic sites present on the $Li_{20}\beta$ zeolite withdraw the primary hydroxy group of GLY and at the same time they accompany the interaction between the O of DMC and Si present on the surface of the catalyst. Moreover, DMC gets triggered by the Lewis acidic sites of Si present in zeolite. Furthermore, the carbonyl group present on DMC was nucleophilically attacked by the primary hydroxy group of GLY, followed by alcohol elimination to form an intermediate.[54] The intermediate undergoes intramolecular nucleophilic substitution to synthesize GC by eliminating another alcohol molecule.

6. Conclusion

In the present work, zeolite beta was successfully modified with different alkali and alkaline earth metals using the wet-impregnation

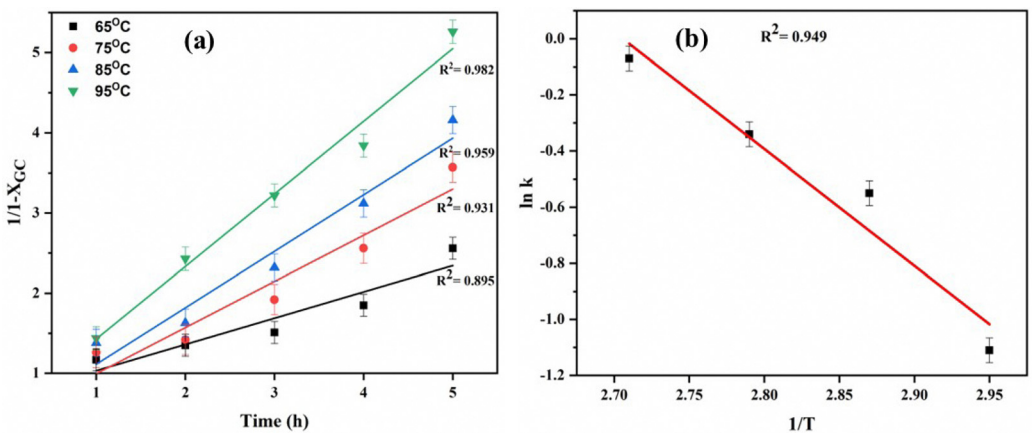

Fig. 16 (a) A plot of $1/(1 - X_{GC})$ *vs.* reaction time for the transesterification reaction and (b) $\ln k$ *vs.* $1/T$ plot for transesterification of GLY with DMC.

method. Under optimal reaction conditions (GLY : DMC, 1 : 5; catalyst dosage, 10 wt% w.r.t. GLY; temperature, 95 °C; time, 5 h), $Li_{20}\beta$ zeolite became the optimum catalyst for the transesterification reaction. A maximum GC yield of 81.48% was observed and the reaction showed second-order reaction kinetics having an activation energy of 34.60 kJ mol^{-1}. The stability and performance of $Li_{20}\beta$ were examined by reusing it for five reaction cycles, which showed a decrease in the GC yield of 59.9% but imparting 100% selectivity towards GC.

Conflicts of interest

There is no conflict of interest to declare.

Acknowledgements

All the authors would like to thank Thapar Institute of Engineering and Technology, Patiala, Punjab for financial support.

References

1 S. Nomanbhay, R. Hussein and M. Y. Ong, *Green Chem. Lett. Rev.*, 2018, **11**, 135–157.
2 N. Rozulan, S. A. Halim, N. Razali and S. S. Lam, *Biomass Convers. Biorefinery*, 2022, **12**, 4665–4682.
3 L. C. Meher, D. Vidya Sagar and S. N. Naik, *Renewable Sustainable Energy Rev.*, 2006, **10**, 248–268.
4 Z. Ullah, M. A. Bustam and Z. Man, *Renew. Energy*, 2015, **77**, 521–526.
5 S. Sahar, S. Sadaf, J. Iqbal, I. Ullah, H. N. Bhatti, S. Nouren, Habib-ur-Rehman, J. Nisar and M. Iqbal, *Sustain. Cities Soc.*, 2018, **41**, 220–226.
6 N. Mansir, S. H. Teo, I. Rabiu and Y. H. Taufiq-Yap, *Chem. Eng. J.*, 2018, **347**, 137–144.
7 C. Delesma, P. Okoye, M. Castellanos-López, A. Longoria and J. Muñiz, *Fuel*, 2022, **307**, 121874.
8 J. Li and T. Wang, *J. Chem. Thermodyn.*, 2011, **43**, 731–736.
9 W. Praikaew, W. Kiatkittipong, F. Aiouache, V. Najdanovic-Visak, M. Termtanun, J. W. Lim, S. S. Lam, K. Kiatkittipong, N. Laosiripojana, S. Boonyasuwat and S. Assabumrungrat, *Int. J. Energy Res.*, 2022, **46**, 1646–1658.
10 D. Procopio and M. L. Di Gioia, *Catalysts*, 2022, **12**, 50.
11 J. Keogh, G. Deshmukh and H. Manyar, *Fuel*, 2022, **310**, 122484.
12 K. Abida, B. Chudasama and A. Ali, *New J. Chem.*, 2020, **44**, 9365–9376.
13 A. Kaur and A. Ali, *Ind. Eng. Chem. Res.*, 2020, **59**, 2667–2679.
14 W. K. Teng, G. C. Ngoh, R. Yusoff and M. K. Aroua, *Energy Convers. Manage.*, 2014, **88**, 484–497.
15 S. Nomanbhay, M. Y. Ong, K. W. Chew, P. L. Show, M. K. Lam and W. H. Chen, *Energies*, 2020, **13**, 1483.
16 J. R. Ochoa-Gómez, O. Gómez-Jiménez-Aberasturi, C. Ramírez-López and M. Belsué, *Org. Process Res. Dev.*, 2012, **16**, 389–399.
17 A. Galadima and O. Muraza, *Waste Biomass Valorization*, 2017, **8**, 141–152.
18 M. O. Sonnati, S. Amigoni, E. P. Taffin De Givenchy, T. Darmanin, O. Choulet and F. Guittard, *Green Chem.*, 2013, **15**, 283–306.
19 P. U. Okoye, A. Z. Abdullah and B. H. Hameed, *Energy Convers. Manage.*, 2017, **133**, 477–485.
20 G. Rokicki, P. Rakoczy, P. Parzuchowski and M. Sobiecki, *Green Chem.*, 2005, **7**, 529–539.
21 F. Paquin, J. Rivnay, A. Salleo, N. Stingelin and C. Silva, *J. Mater. Chem. C*, 2015, **3**, 10715–10722.
22 Z. I. Ishak, N. A. Sairi, Y. Alias, M. K. T. Aroua and R. Yusoff, *Catal. Rev.: Sci. Eng.*, 2017, **59**, 44–93.
23 A. O. Esan, A. D. Adeyemi and S. Ganesan, *J. Cleaner Prod.*, 2020, **257**, 120561.
24 M. Manikandan and P. Sangeetha, *ChemistrySelect*, 2019, **4**, 6672–6678.
25 F. Paquin, J. Rivnay, A. Salleo, N. Stingelin and C. Silva, *J. Mater. Chem. C*, 2015, **3**, 10715–10722.
26 W. Roschat, S. Phewphong, T. Kaewpuang and V. Promarak, *Mater. Today Proc.*, 2018, **5**, 13909–13915.
27 X. Zhang, S. Wei, X. Zhao, Z. Chen, H. Wu, P. Rong, Y. Sun, Y. Li, H. Yu and D. Wang, *Appl. Catal., A*, 2020, **590**, 117313.
28 G. Pradhan and Y. C. Sharma, *Fuel*, 2021, **284**, 118966.
29 L. Zheng, S. Xia, X. Lu and Z. Hou, *Cuihua Xuebao*, 2015, **36**, 1759–1765.
30 M. Malyaadri, K. Jagadeeswaraiah, P. S. Sai Prasad and N. Lingaiah, *Appl. Catal., A*, 2011, **401**, 153–157.
31 G. Parameswaram, P. S. N. Rao, A. Srivani, G. N. Rao and N. Lingaiah, *Mol. Catal.*, 2018, **451**, 135–142.
32 Y. Li, H. Zhao, W. Xue, F. Li and Z. Wang, *Nanomaterials*, 2022, **12**, 1972.
33 S. E. Kondawar, C. R. Patil and C. V. Rode, *ACS Sustainable Chem. Eng.*, 2017, **5**, 1763–1774.
34 P. Zhang, Y. Chen, M. Zhu, C. Yue, Y. Dong, Y. Leng, M. Fan and P. Jiang, *Catal. Lett.*, 2020, **150**, 2863–2872.
35 A. Chotchuang, P. Kunsuk, A. Phanpitakkul, S. Chanklang, M. Chareonpanich and A. Seubsai, *Catal. Today*, 2022, **388–389**, 351–359.
36 S. Wang, P. Hao, S. Li, A. Zhang, Y. Guan and L. Zhang, *Appl. Catal., A*, 2017, **542**, 174–181.
37 P. U. Okoye, S. Wang, L. Xu, S. Li, J. Wang and L. Zhang, *Energy Convers. Manage.*, 2019, **179**, 192–200.
38 P. Devi, U. Das and A. K. Dalai, *Chem. Eng. J.*, 2018, **346**, 477–488.
39 S. Bepari, N. C. Pradhan and A. K. Dalai, *Catal. Today*, 2017, **291**, 36–46.
40 S. Arora, V. Gosu and V. Subbaramaiah, *Mol. Catal.*, 2020, **496**, 111188.
41 S. Arora, V. Gosu, V. Subbaramaiah and T. C. Zhang, *Can. J. Chem. Eng.*, 2021, 1868–1883.
42 Y. T. Algoufi and B. H. Hameed, *Fuel Process. Technol.*, 2014, **126**, 5–11.
43 A. V. Shvydko, S. A. Prihod'ko and M. N. Timofeeva, *Catal. Ind.*, 2022, **14**, 181–188.

44 S. Pan, L. Zheng, R. Nie, S. Xia, P. Chen and Z. Hou, *Cuihua Xuebao*, 2012, **33**, 1772–1777.
45 P. U. Okoye, A. Z. Abdullah and B. H. Hameed, *J. Taiwan Inst. Chem. Eng.*, 2016, **68**, 51–58.
46 Y. T. Algoufi, U. G. Akpan, G. Kabir, M. Asif and B. H. Hameed, *Energy Convers. Manage.*, 2017, **138**, 183–189.
47 N. Hindryawati, G. P. Maniam, M. R. Karim and K. F. Chong, *Eng. Sci. Technol. Int. J.*, 2014, **17**, 95–103.
48 H. Maleki, M. Kazemeini, A. S. Larimi and F. Khorasheh, *J. Ind. Eng. Chem.*, 2017, **47**, 399–404.
49 Z. Liu, B. Li, F. Qiao, Y. Zhang, X. Wang, Z. Niu, J. Wang, H. Lu, S. Su, R. Pan, Y. Wang and Y. Xue, *ACS Omega*, 2022, **7**, 5032–5038.
50 Z. Liu, J. Wang, M. Kang, N. Yin, X. Wang, Y. Tan and Y. Zhu, *J. Ind. Eng. Chem.*, 2015, **21**, 394–399.
51 X. Song, Y. Wu, F. Cai, D. Pan and G. Xiao, *Appl. Catal., A*, 2017, **532**, 77–85.
52 S. Arora, V. Gosu, U. K. A. Kumar and V. Subbaramaiah, *J. Cleaner Prod.*, 2021, **295**, 126437.
53 S. Arora, V. Gosu, V. Subbaramaiah and B. H. Hameed, *J. Environ. Chem. Eng.*, 2021, **9**, 105999.
54 J. X. Wang, K. T. Chen, J. S. Wu, P. H. Wang, S. T. Huang and C. C. Chen, *Fuel Process. Technol.*, 2012, **104**, 167–173.
55 W. A. Khanday, P. U. Okoye and B. H. Hameed, *Energy Convers. Manage.*, 2017, **151**, 472–480.
56 S. Sahani, S. N. Upadhyay and Y. C. Sharma, *Ind. Eng. Chem. Res.*, 2021, **60**, 67–88.
57 G. Jaya Rao, R. Mazumder, D. Dixit, C. Ghoroi, S. Bhattacharyya and P. Chaudhuri, *Ceram. Int.*, 2019, **45**, 4022–4034.
58 M. L. Kantam, B. P. C. Rao, B. M. Choudary, K. K. Rao, B. Sreedhar, Y. Iwasawa and T. Sasaki, *J. Mol. Catal. A: Chem.*, 2006, **252**, 76–84.
59 L. Feng, Y. Gong, M. Yang, Y. Shi, X. Xiang, J. Wei and T. Lu, *Mater. Manuf. Process.*, 2018, **33**, 99–103.
60 B. Philippe, R. Dedryvère, J. Allouche, F. Lindgren, M. Gorgoi, H. Rensmo, D. Gonbeau and K. Edström, *Chem. Mater.*, 2012, **24**, 1107–1115.
61 P. Gautam, S. Barman and A. Ali, *ChemistrySelect*, 2022, **7**, 1–9.

